Inorganic Chemistry

Article

pubs.acs.org/IC

Synthesis and Characterization of the $LiMnBO_3$–$LiCoBO_3$ Solid Solution and Its Use as a Lithium-Ion Cathode Material

Barbara Le Roux,[†,‡,§] Carole Bourbon,[†,‡] Oleg I. Lebedev,[§] Jean-François Colin,*[,†,‡] and Valerie Pralong[§]

[†]Université de Grenoble Alpes, F-38000 Grenoble, France

[‡]CEA, LITEN, LCB, 17 rue des Martyrs, F-38054 Grenoble Cedex 9, France

[§]Laboratoire de Cristallographie et Sciences des Matériaux, CRISMAT, ENSICAEN, Université de Caen, CNRS, 6 Bd Maréchal Juin, 14050 Caen, France

ABSTRACT: A complete solid solution of *m*-$Li(Mn_{1-x}Co_x)BO_3$ has been successfully synthesized for the first time with the idea of improving the average potential versus *m*-$LiMnBO_3$. These compounds have been obtained by a multiple-step process. Interestingly, transmission electron microscopy results indicate that the $C2/c$ space group previously reported for *m*-$LiMBO_3$ (M = Mn, Co) cannot describe *m*-$Li(Mn_{1-x}Co_x)BO_3$ compounds. Each material shows electrochemical activity, without in situ carbon coating. Despite a large polarization, we report a capacity of almost 60 mAh/g at the first discharge at $C/20$ rate with good stability up to five cycles for $LiMn_{0.7}Co_{0.3}BO_3$.

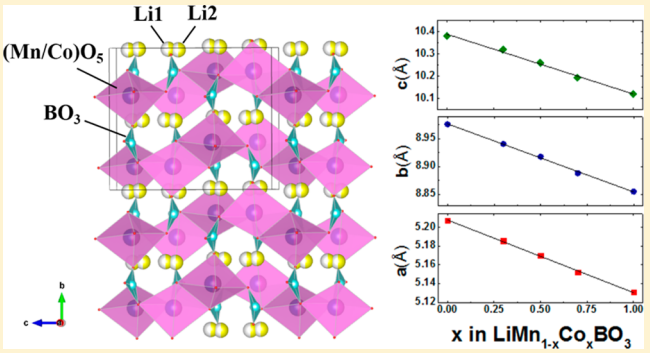

INTRODUCTION

Because the inductive effect was shown by Goodenough's group,[1,2] compounds with a polyanionic framework were considered as possible electrode materials with the very interesting property that the operating voltage can be tuned by changing the polyanion or the transition metal.[3] Among these materials, the phosphate $LiFePO_4$ received much attention especially for its safety and low cost.[4] However, its specific capacity is limited to 170 mAh/g, which will limit its energy density to 586 Wh/kg (with an average potential at 3.45 V). $LiMBO_3$ borate compounds (M = Fe, Mn, Co) could be good alternatives to phosphates by having a higher theoretical specific capacity (>210 mAh/g) because of their lightest $(BO_3)^{3-}$ polyanionic groups and keeping the advantage of safety. Also, even if the lithium intercalation potentials are lower in these compounds (~0.4 V vs $LiMPO_4$), the energy density is expected to be higher than that in phosphates.[5] Moreover, borate compounds are expected to suffer from very low volume change upon cycling, which is very interesting for the cycle life of the battery.[5]

These materials exist under different polymorphs: one described in monoclinic $C2/c$ symmetry (M = Fe, Mn, Co), and the other one described in the hexagonal $P\bar{6}$ space group (M = Mn), which will be obtained at higher temperature. These compounds were first considered as positive electrode materials in 2001 by Legagneur (excepted for *m*-$LiMnBO_3$), who showed their electrochemical activities but with very limited reversible capacities probably because of their low ionic and electronic conductivities.[6] Concerning the monoclinic $LiMnBO_3$ polymorph, Ceder et al. demonstrated its electrochemical activity with a second discharge capacity of 100 mAh/g at $C/20$ with carbon coating.[7] Since then, different attempts have been made to improve the performances of this phase, but there has been no significant change in terms of the obtained reversible capacity. Recently, Yamashita et al. improved the reversible capacity of $LiCoBO_3$ to 30 mAh/g at $C/20$ and showed that the electrochemical activity is centered at 4 V in this compound.[8] A sol–gel synthesis developed by Afyon et al. allowed them to obtain around 45 mAh/g at the first discharge at $C/20$ with the use of reduced graphite oxide.[9] However, reaching the theoretical capacity of this compound seems difficult because of the limitations induced by the structural/chemical instability of fully delithiated $LiCoBO_3$ and the stability window of the electrolytes.[8] Concerning $LiFeBO_3$, Yamada et al. nearly achieved its theoretical capacity (190 mAh/g at $C/20$) by reducing the particle size and paying careful attention to surface poisoning by air.[10] However, because the redox potential generated by $Fe^{3+/}Fe^{2+}$ in the $LiFeBO_3$ compound is relatively low (around 3 V vs Li^6), *m*-$LiMn_{0.5}Fe_{0.5}BO_3$ was investigated by Abouimrane et al. to increase the overall potential versus $LiFeBO_3$.[11] Then, Yamada et al. synthesized the complete solid solution *m*-$Li(Mn_xFe_{1-x})BO_3$ and obtained a first discharge capacity of 140 mAh/g at $C/20$ (between 1.5 and 4.5 V) for the *m*-$LiMn_{0.5}Fe_{0.5}BO_3$/C compound.[12]

In this paper, we report the synthesis and electrochemical activity of the $Li(Mn_{1-x}Co_x)BO_3$ complete solid solution for the first time. These materials have been synthesized with the idea of enhancing the overall potential versus $LiMnBO_3$. Indeed, $Li(Mn_{1-x}Co_x)BO_3$ compounds could be good

Received: February 3, 2015
Published: May 19, 2015

DOI: 10.1021/acs.inorgchem.5b00260
Inorg. Chem. 2015, 54, 5273–5279

alternatives to having both a reversible capacity and a relatively high voltage. Moreover, because there is no iron in these compounds, they are expected to be less sensitive to surface poisoning by air than *m*-Li($Mn_{1-x}Fe_x$)BO_3.

EXPERIMENTAL SECTION

The compounds were characterized by powder X-ray diffraction (XRD) using a Bruker D8 diffractometer equipped with Bragg–Brentano geometry (Cu $K\alpha_{1,2}$ radiation). *Fullprof* software was used for full-pattern matching and Rietveld refinements.

Simultaneous inductively coupled plasma optical emission spectroscopy (ICP-OES; Agilent 725 series) was used to determine the quantity of metals in our compounds. Before analysis, each material was diluted with HNO_3.

Transmission electron microscopy (TEM), including electron diffraction (ED) and high-resolution TEM (HRTEM), studies were carried out on crushed samples, suspended in butanol, and deposited on a holey carbon copper grid inside an argon-filled glovebox, using a Tecnay G2 30 UT microscope operated at 300 kV and having 0.17 nm point resolution equipped with an EDAX detector for EDX analysis. The low-dose intensity beam regime was used for TEM in order to minimize electron-beam damage of the structure inside the microscope. HRTEM image simulation was performed using *CrystalKit* and *MacTempas* software. Scanning electron microscopy (SEM) images were collected on a LEO 1530 high-resolution microscope.

Electrochemistry characterization of each material was performed in coin cells (CR2032 type). Before being formulated, each material was ball-milled (85 wt %) with 15 wt % Ketjen Black carbon for 4 h at 500 rpm with a planetary ball milling (Retsch). The positive electrodes were prepared by mixing this composite with 10 wt % poly(vinylidene fluoride) (PVDF) using *N*-methylpyrrolidone as a solvent. So, the electrode is composed of 76.5 wt % active material, 13.5 wt % Ketjen Black carbon, and 10 wt % PVDF. Each electrode contained about 3–4 mg of active material and had a diameter of 14 mm. Cell assembly was carried out in an argon-filled glovebox. Lithium metal foil was used as the negative electrode and 1 M $LiPF_6$ dissolved in a mixture of ethylene carbonate/propylene carbonate/dimethyl carbonate (1:1:3) as the electrolyte (LP100, Powerlyte). A porous propylene film (Celgard 2400) and a polyolefin film (Viledon) were used as separators.

The charge–discharge characteristics were examined over a voltage range of 1.8–4.7 V versus Li^+/Li at a constant rate of *C*/20 (corresponding to a theoretical exchange of one electron per formula during charging or discharging for 20 h). Cyclic voltammetry was also carried out between 2 and 4.7 V at 0.05 and 0.009 mV/s. Electrochemical studies were carried out at room temperature using an Arbin battery cycler for galvanostatic cycling and a VSP (BioLogic) for cyclic voltammetry.

RESULTS AND DISCUSSION

Solid-State Synthesis of Monoclinic Li($Mn_{1-x}Co_x$)BO_3. The series Li($Mn_{1-x}Co_x$)BO_3 was synthesized by a multiple-step process involving the synthesis of orthoborates $M_3(BO_3)_2$ (M = Mn, Co). First, each orthoborate was synthesized separately with a procedure close to the one used by Belkébir et al. to synthesize $Co_2B_2O_5$.[13] To obtain $Co_3(BO_3)_2$, B_2O_3 and $CoC_2O_4{\cdot}2H_2O$ were ball-milled and heated at 800 °C for 6 h in air (+5/−10 °C/min). For $Mn_3(BO_3)_2$, B_2O_3 and $MnC_2O_4{\cdot}2H_2O$ were also ball-milled for 5 h at 500 rpm before being heated at 700 °C for 6 h in an argon atmosphere (+5/−10 °C/min). A mixture of $Mn_3(BO_3)_2$ and $Mn(BO_2)_2$ was obtained. Then, this mixture and/or $Co_3(BO_3)_2$ were mixed with Li_2CO_3 and H_3BO_3 for 5 h at 500 rpm before being heated at 500 °C for 6 h under an argon atmosphere (+5/−20 °C/min). Different mixtures were made to obtain the series Li($Mn_{1-x}Co_x$)BO_3.

The use of intermediate $M_3(BO_3)_2$ is needed to synthesize Li($Mn_{1-x}Co_x$)BO_3 because of the easy formation of metallic cobalt under argon at high temperature and the oxidation of manganese during heat treatment carried out under air. Indeed, a one-step process with a heat treatment under argon leads to the synthesis of *m*-$LiMnBO_3$ and metallic cobalt.

Powder XRD patterns of Li($Mn_{1-x}Co_x$)BO_3 (with x = 0, 0.3, 0.5, 0.7, and 1) are shown in Figure 1.

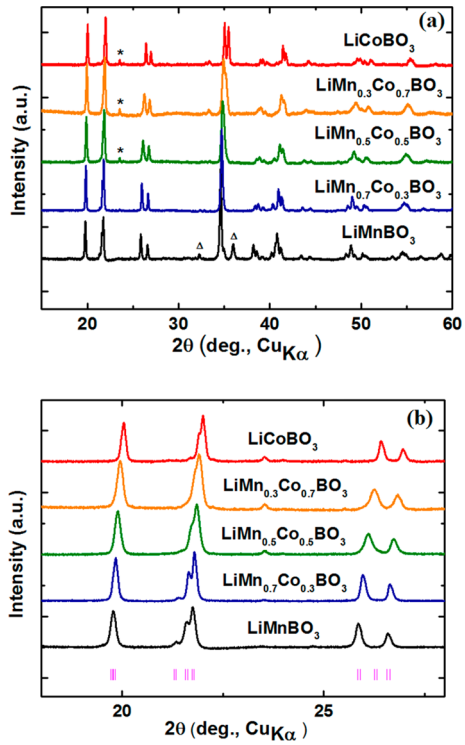

Figure 1. Powder XRD patterns of (a) Li($Mn_{1-x}Co_x$)BO_3 (Δ, $Mn_3(BO_3)_2$; *, Li_6CoO_4 impurity) and (b) an enlargement of the 18–28° zone showing the [110], [020], [−111], [021], [111], [−112], [022], and [112] reflections.

The monoclinic structure is maintained, and there is a continuous shift of the diffraction peaks to higher angle with the insertion of cobalt in the structure. Some remaining $Mn_3(BO_3)_2$ is detected for *m*-$LiMnBO_3$ as well as a Li_6CoO_4 impurity for compositions with $x \geq 0.5$. The refined lattice parameters are summarized in Table 1.

The lattice parameters of each material were refined through a whole pattern matching method with *C*2/*c* symmetry. Parameters obtained for *m*-$LiMnBO_3$ and $LiCoBO_3$ are in good agreement with the literature.[14,8] The evolution of the lattice parameters of Li($Mn_{1-x}Co_x$)BO_3 shows a linear dependence on the cobalt content x, following Vegard's law, confirming that Li($Mn_{1-x}Co_x$)BO_3 ($0 \leq x \leq 1$) forms a complete solid solution (Figure 2). ICP results presented in Table 2 are consistent with the expected formula.

The crystal structure of *m*-$LiMBO_3$ (M = Mn, Co) is shown in Figure 3a. It is built from unusual edge-sharing MO_5 trigonal bipyramids running along the [−101] direction. These ribbons are connected through planar-triangular BO_3 groups by corner sharing. In this framework, one lithium is linked to four oxygen atoms and will diffuse along the *c* axis.

Different models have been proposed for the structure of *m*-$LiMnBO_3$. The first one has been described by Bondareva et al.

DOI: 10.1021/acs.inorgchem.5b00260
Inorg. Chem. 2015, 54, 5273–5279

Table 1. Refined Lattice Parameters of $Li(Mn_{1-x}Co_x)BO_3$

formula	a (Å)	b (Å)	c (Å)	β (deg)	V (Å^3)	χ^2
$LiMnBO_3$	5.207(1)	8.976(1)	10.381(1)	91.83(1)	484.9(1)	3.0
$LiMn_{0.7}Co_{0.3}BO_3$	5.186(1)	8.941(1)	10.321(1)	91.69(1)	478.3(1)	3.5
$LiMn_{0.5}Co_{0.5}BO_3$	5.170(1)	8.918(1)	10.260(1)	91.59(1)	472.9(1)	2.6
$LiMn_{0.3}Co_{0.7}BO_3$	5.152(1)	8.888(1)	10.194(1)	91.44(1)	466.6(1)	2.1
$LiCoBO_3$	5.131(1)	8.855(1)	10.120(1)	91.32(1)	459.9(1)	3.0

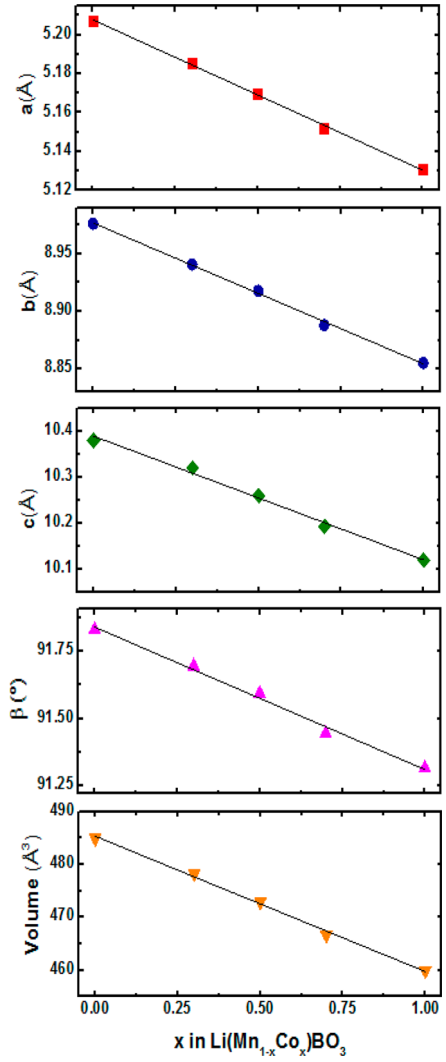

Figure 2. Evolution of the lattice parameters of $Li(Mn_{1-x}Co_x)BO_3$ against the cobalt content x.

Table 2. Atomic Ratio of Metals in $Li(Mn_{1-x}Co_x)BO_3$ Determined by ICP-OES

	Li	Mn	Co
$LiMnBO_3$	0.89	1.00	0.00
$LiMn_{0.7}Co_{0.3}BO_3$	0.97	0.73	0.27
$LiMn_{0.5}Co_{0.5}BO_3$	0.99	0.54	0.46
$LiMn_{0.3}Co_{0.7}BO_3$	1.05	0.33	0.67
$LiCoBO_3$	1.07	0.00	1.00

with two close positions for the lithium and two close positions for the manganese ("2Li 2Mn").[15] This model has also been used by Kim et al. with the same positions but with different occupancies for lithium and oxygen atoms, suggesting local disordering.[7] More recently, Tao et al. proposed another model

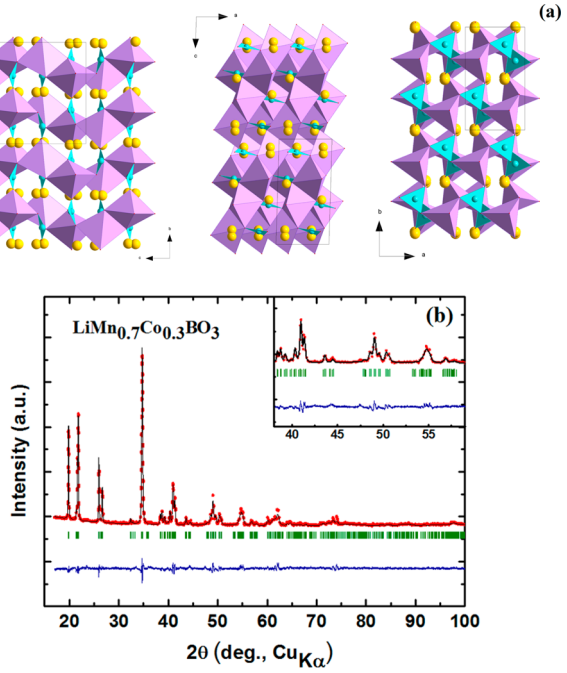

Figure 3. (a) Structure of $Li(Mn_{1-x}Co_x)BO_3$. The yellow, purple, and blue colors indicate lithium, M (M = Mn, Co), and boron atoms, respectively, and their oxygen polyhedra. (b) Rietveld refinement of $LiMn_{0.7}Co_{0.3}BO_3$. R_p= 20.9% and R_{wp} = 12.9%. The red dots correspond to experimental data, and the black line is the calculated fit. The bottom curve is the difference of the patterns, $y_{obs} - y_{cal}$, and the green sticks indicate the angular positions of the allowed Bragg reflections.

with two positions for the lithium and only one for the manganese ("2Li 1Mn").[14] Concerning $LiCoBO_3$, Piffard et al. first proposed a model for the atomic positions in 1998.[16] In this one, there are two sites for the lithium and two sites for the cobalt. However, recently, Tao et al. also used his "2Li 1M" cation distribution model to describe $LiCoBO_3$[14] (and $LiFeBO_3$[17]).

In the first part of our study, we also used a "2Li 1M" cation distribution model to describe $Li(Mn_{1-x}Co_x)BO_3$ compounds. Indeed, there is no evidence of a second site for M because no asymmetry is observed in the remaining density in the difference Fourier map with the "2Li 1M" model. The Rietveld refinement results for $Li(Mn_{0.7}Co_{0.3})BO_3$ are given in Figure 3b. This refinement has been made based on the $C2/c$ space group. The resolution of experimental data was not high enough to refine B_{iso}, so we have used fixed plausible values. The occupancy was not refined either because of the very close electronic density of cobalt and manganese (we have used theoretical values; Table 3).

In the MO_5 trigonal bipyramids of $Li(Mn_{0.7}Co_{0.3})BO_3$, the M−O distances range from 2.058 to 2.283 Å, with three short ones that form a triangle perpendicular to [001]. These

DOI: 10.1021/acs.inorgchem.5b00260
Inorg. Chem. 2015, 54, 5273−5279

Table 3. Positional Parameters of $LiMn_{0.7}Co_{0.3}BO_3$ in the *C*2/*c* Space Group

atom	occupancy	*x*	*y*	*z*
Mn	0.7	0.16295(3)	0.33493(3)	0.12515(2)
Co	0.3	0.16295(3)	0.33493(3)	0.12515(2)
Li1	0.5	0.66201(7)	0.50720(3)	0.17320(3)
Li2	0.5	0.65810(4)	0.51230(3)	0.11101(2)
B	1.0	0.16552(2)	0.67071(1)	0.12360(1)
O1	1.0	0.40377(1)	0.15632(9)	0.09427(5)
O2	1.0	0.76234(1)	0.30719(6)	0.16191(5)
O3	1.0	0.33064(1)	0.54786(5)	0.12692(5)

bipyramids are elongated along [001] (2.235 and 2.283 Å). The B−O distances range from 1.373 to 1.392 Å, which is quite common in borate compounds with BO_3 groups. Li-$(Mn_{1-x}Co_x)BO_3$ compounds ($0 \leq x \leq 1$) only differ by the size of the MO_5 trigonal bipyramid (Table 4).

Table 4. Interatomic Distances (Å) in $LiMn_{0.7}Co_{0.3}BO_3$

B1−O1	1.3876	Li1−O1	2.0183
B1−O2	1.3732	Li1−O2	1.8669
B1−O3	1.3924	Li1−O3	2.0952
M1−O1	2.2835	Li1−O1	1.8065
M1−O2	2.1368	Li2−O1	1.8230
M1−O1	2.0577	Li2−O2	1.9785
M1−O2	2.2354	Li2−O3	2.5177
M1−O3	2.0927	Li2−O1	1.7398

In order to confirm the structure of $Li(Mn_{0.7}Co_{0.3})BO_3$, TEM was applied. ED patterns of $Li(Mn_{0.7}Co_{0.3})BO_3$ shown in Figure 4a are in good agreement with the basis of the proposed monoclinic structure β, and unit cell parameters calculated with ED patterns are close to the refined values presented in Figure 2a. However, extinction conditions obtained from the experimental ED patterns are not completely consistent with the *C*2/*c* (No. 15) space group, in particular *h*0*l* with $l = 2n$, suggesting a lower-symmetry space group. Structural analysis revealed that observed extinction conditions better fit with the *C*2 (No. 5) space group. Atomic positions for $Li(Mn_{0.7}Co_{0.3})BO_3$ recalculated in *C*2 (No. 5) symmetry are presented in Table 5. No actual difference was found in the XRD Rietveld refinement with the *C*2/*c* or *C*2 space group. Neutron diffraction is planned to completely resolve the structure.

Therefore, the ED patterns of $Li(Mn_{0.7}Co_{0.3})BO_3$ taken along the main zone axis are shown in Figure 4a and can be completely indexed based on the monoclinic *C*2 (No. 15) structure with the following unit cell parameters: $a \sim 5.2$ Å, $b \sim 9$ Å, and $c \sim 10$ Å. In order to confirm the structure of $Li(Mn_{0.7}Co_{0.3})BO_3$, a HRTEM study was performed. Figure 4b shows the HRTEM image of $Li(Mn_{0.7}Co_{0.3})BO_3$ taken along the [110] zone axis. It should be notice that material is sensitive to the electron beam and some structure transformation during the experiment can occur inside the microscope. However, the Fourier transform (FT) pattern taken from the HRTEM image (Figure 4b, inset) exhibits similar to [110] ED pattern spot distribution, suggesting that the basis of the structure remained intact. The [110] HRTEM image shows rows of brighter dots running along the *a* axis and spaced by ~10 Å in the *c* direction that alternate with strips of less bright spots. Bearing in mind the previous structural analysis and image simulation, (Mn, Co) atoms correspond to black dots and the strips of less bright

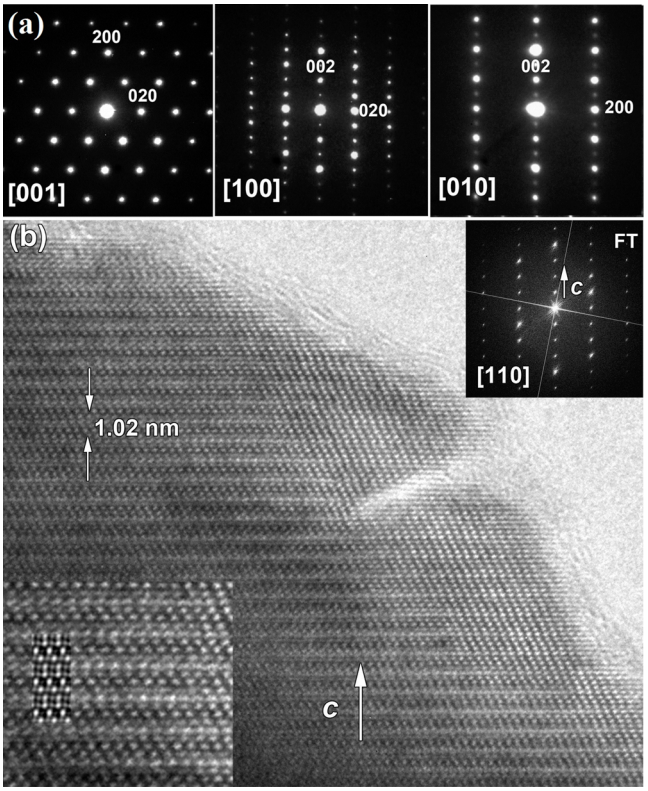

Figure 4. (a) ED patterns of the $LiMn_{0.7}Co_{0.3}BO_3$ sample recorded at room temperature along the main zone axis: [001], [100], and [010]. (b) [110] HRTEM image of $LiMn_{0.7}Co_{0.3}BO_3$ and the corresponding FT pattern given in the inset. The calculated image based on the structure parameters shown in Table 5 is given in the inset ($\Delta f = -15$ nm; $t = 5$ nm).

Table 5. Positional Parameters of $LiMn_{0.7}Co_{0.3}BO_3$ in the *C*2 Space Group

atom	occupancy	*x*	*y*	*z*
Mn1	0.7	0.16295(3)	0.33493(3)	0.37515(2)
Co1	0.3	0.16295(3)	0.33493(3)	0.37515(2)
Li1	0.5	0.66201(7)	0.50720(3)	0.42320(3)
Li2	0.5	0.65810(4)	0.51230(3)	0.36101(2)
B1	1.0	0.16552(2)	0.67071(1)	0.37360(2)
O1	1.0	0.40377(1)	0.15632(9)	0.34427(1)
O2	1.0	0.76234(1)	0.30719(6)	0.41191(5)
O3	1.0	0.33064(1)	0.54786(5)	0.37692(5)
Mn2	0.7	0.33705(3)	0.16507(3)	0.12485(2)
Co2	0.3	0.33705(3)	0.16507(3)	0.12485(2)
Li1	0.5	0.33799(7)	0.49280(3)	0.07680(3)
Li2	0.5	0.34190(4)	0.48770(3)	0.13899(2)
B2	1.0	0.83448(2)	0.32929(1)	0.12640(2)
O4	1.0	0.09623(1)	0.34368(9)	0.15573(1)
O5	1.0	0.73766(1)	0.19281(6)	0.08809(5)
O6	1.0	0.66936(1)	0.45214(5)	0.12308(5)

spots represent stacking of the $[M-O-]_\infty$ ribbons, which are running along the *c* axis and are MO_5 bipyramids thick. According to the image simulation (Figure4a, inset), the bright dots correspond to the channels and the dark dots to the columns of heavy atoms.

Electrochemical Tests of Monoclinic $Li(Mn_{1-x}Co_x)BO_3$. The galvanostatic charge−discharge curves of the series $Li(Mn_{1-x}Co_x)BO_3$ and the evolution of the specific reversible

DOI: 10.1021/acs.inorgchem.5b00260
Inorg. Chem. 2015, 54, 5273−5279

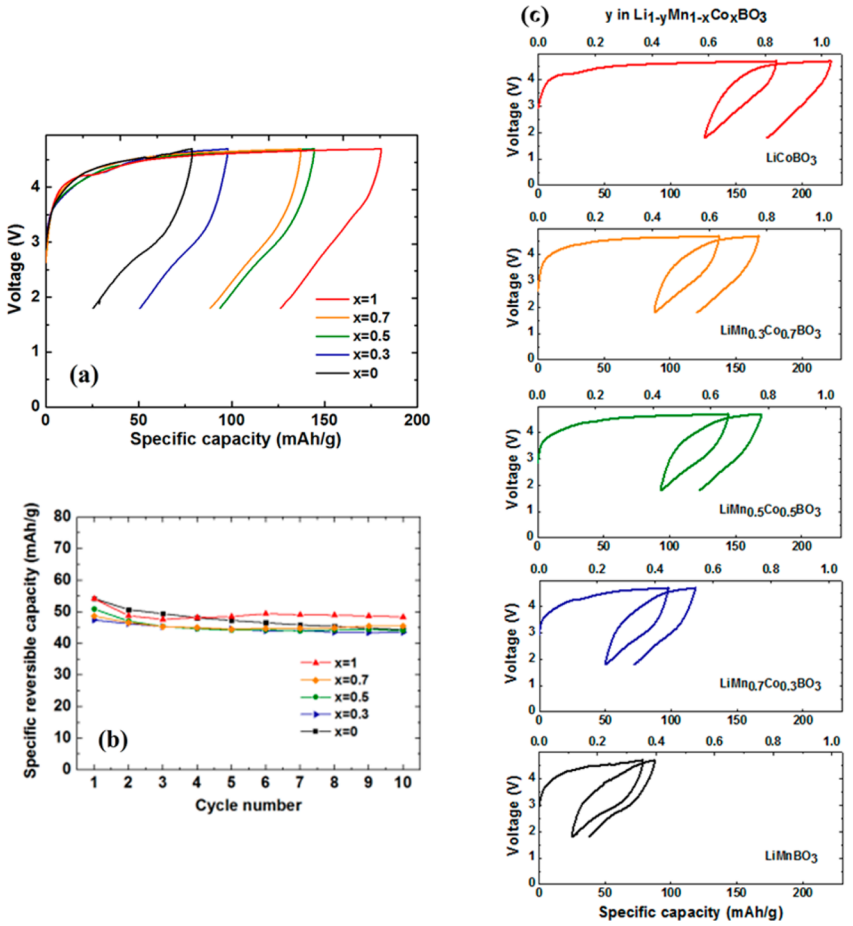

Figure 5. (a) First galvanostatic charge−discharge curves at *C*/20 rate of the series $Li(Mn_{1-x}Co_x)BO_3$. (b) Evolution of the specific reversible capacity upon cycling between 1.8 and 4.7 V. (c) First and second charge−discharge curves at *C*/20 rate of the series $Li(Mn_{1-x}Co_x)BO_3$.

capacity upon cycling are shown in Figure 5. Measurements were made at room temperature at a constant rate of *C*/20 between 1.8 and 4.7 V. All compounds show electrochemical activity but with high polarization probably because of their low electronic conductivity.[5,18] It seems that the charge capacity tends to increase with the cobalt content to reach 180 mAh/g for $LiCoBO_3$ (for x = 0.5 and 0.7, the charge capacities are close). However, a large part of the charge capacity obtained for compounds with cobalt is irreversible because there is no significant difference between each material in terms of the reversible capacity at the first discharge, which is between 48 and 54 mAh/g. This extra capacity may come from the reaction with the electrolyte, which seems to be more pronounced with the compound containing cobalt. This may also be due to the fact that the charged state of $LiCoBO_3$ was found to be structurally/chemically instable and prone to decomposition, as has been suggested by Yamada et al.[8] The same phenomenon is observed during the second cycle, where the charge capacity and the irreversible capacity increase with the content of cobalt. However, the discharge profiles remain identical, showing that the same reversible phenomenon is involved. Concerning the similar reversible capacity obtained for all materials, it is likely that it reflects the similar morphology of these materials, as shown by the SEM images on Figure 6. The borates are indeed known to be bad ionic and electronic conductors, and their performances are tightly linked to their particle size.

Cyclic voltammetry curves of the series $Li(Mn_{1-x}Co_x)BO_3$ are presented in Figure 7. For $LiMnBO_3$ and $LiCoBO_3$, the

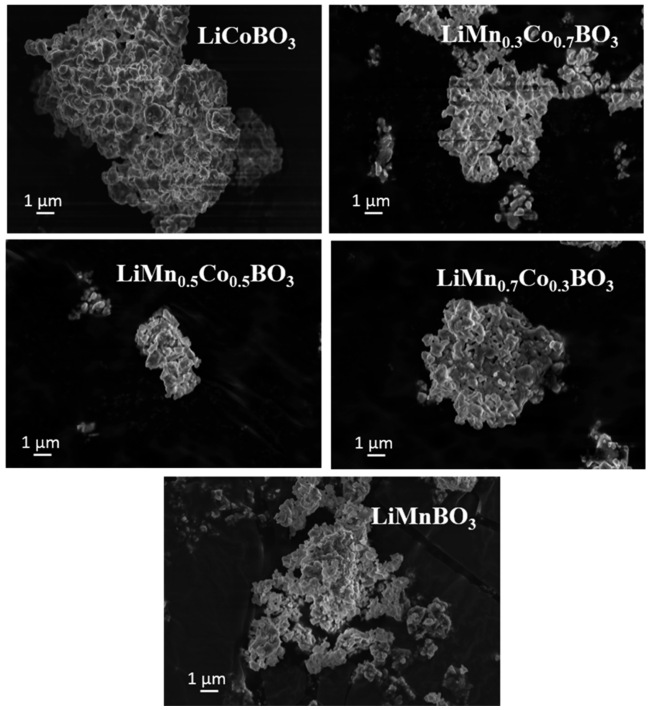

Figure 6. SEM images of the series $Li(Mn_{1-x}Co_x)BO_3$ with different cobalt compositions, showing no significant difference in the morphology of the samples.

DOI: 10.1021/acs.inorgchem.5b00260
Inorg. Chem. 2015, 54, 5273−5279

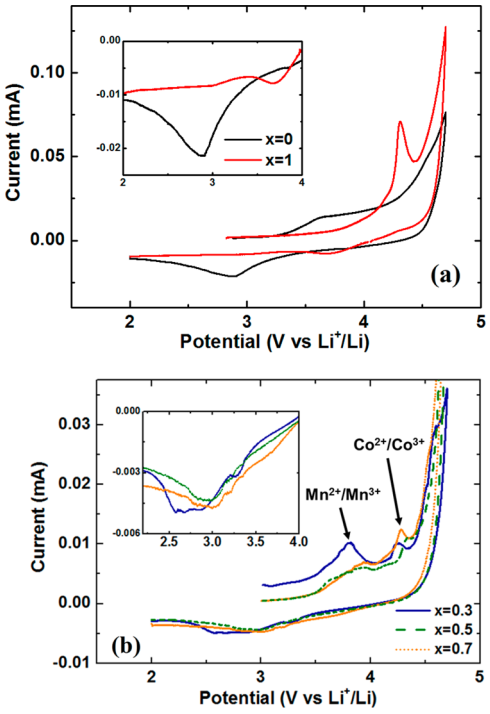

Figure 7. Cyclic voltammetry curves of the series $Li(Mn_{1-x}Co_x)BO_3$ between 2 and 4.7 V (a) at 0.05 mV/s for $LiMnBO_3$ (black) and $LiCoBO_3$ (red) and (b) at 0.009 mV/s for $LiMn_{0.7}Co_{0.3}BO_3$ (blue), $LiMn_{0.5}Co_{0.5}BO_3$ (green), and $LiMn_{0.3}Co_{0.7}BO_3$ (orange).

potential was scanned at 0.05 mV/s, whereas it was slower for other compositions in order to try to distinguish the redox peaks from manganese and cobalt (0.009 mV/s). For $LiMnBO_3$, oxidation begins around 3.5 V and the first discharge exhibits a broad reduction peak centered on 2.8 V. The Co^{3+}/Co^{2+} redox couple is active at higher potential, as is shown by the oxidation peak at 4.2 V and the reduction peak around 3.8 V for the $LiCoBO_3$ compound. For $Li(Mn_{1-x}Co_x)BO_3$ compounds, we clearly observe two oxidation peaks at 3.5 and 4.2 V, showing that both Mn^{3+}/Mn^{2+} and Co^{3+}/Co^{2+} couples are active in these materials. During reduction, the overlapping of the processes makes differentiation more difficult; however, it is clear, from the enlargement, that the working potential shifts to higher potential with higher cobalt content, showing that the cobalt is also active during discharge. Thereby, $Li(Mn_{1-x}Co_x)BO_3$ compounds have higher operating voltage than *m*-$LiMnBO_3$. However, the specific capacity needs to be increased to have better energy density.

Performances obtained for $LiCoBO_3$ are comparable to that reported in the literature with solid-state synthesis and the addition of carbon for the formulation.[8] However, the *m*-$LiMnBO_3$ phase shows poor electrochemical performances compared to that reported, where the first discharge capacity is around 100 mAh/g at *C*/20.[19,20] This is probably due to the large particles obtained by this process, as shown by the SEM images in Figure 6, which leads to poor length path Li^+ diffusion into the material. Moreover, there is no in situ carbon coating during the synthesis, which can prevent particles from being properly electronically connected, and because $LiMBO_3$ borate compounds (M = Fe, Mn, Co) have limited conductivity, that limits their electrochemical performances.[5,18] It is noticeable that, to our knowledge, the state-of-the-art electrochemical performance for an uncoated $LiMnBO_3$ is 58 mAh/g[21] using a broader voltage window of 1−4.8 V versus Li^+/Li, which is very close to the performances obtained by our materials.

Optimized Solid-State Synthesis of Monoclinic $LiMn_{0.7}Co_{0.3}BO_3$. An optimized synthesis has been developed for the $LiMn_{0.7}Co_{0.3}BO_3$ compound in order to decrease the particle size to obtain better performances and also energy and time savings. (This composition has been chosen for its limited irreversible capacity compared to other compositions with cobalt.)

The process has been successfully optimized by reducing the duration of the heat treatment of each step described previously in the initial synthesis. The same precursors have been used and the same ball milling has been done for each step. Then, B_2O_3 and $CoC_2O_4{\cdot}2H_2O$ have been heated at 800 °C under air for only 15 min to obtain $Co_3(BO_3)_2$ (quenching). Similarly, a mixture of $Mn_3(BO_3)_2$ and $Mn(BO_2)_2$ was obtained by heating B_2O_3 and $MnC_2O_4{\cdot}2H_2O$ at 700 °C under argon for 15 min [thermogravimetric analysis made on the precursors and XRD have shown that it is not possible to decrease the temperature of the treatment to obtain $M_3(BO_3)_2$ phases]. Then, this mixture and $Co_3(BO_3)_2$ were ball-milled with Li_2CO_3 and H_3BO_3 for 5 h at 500 rpm before being heated at 500 °C for 1 h under an argon atmosphere. The structure of $Li(Mn_{1-x}Co_x)$-BO_3 was obtained with an optimized process, as shown by the XRD pattern presented in Figure 8a. However, the lattice

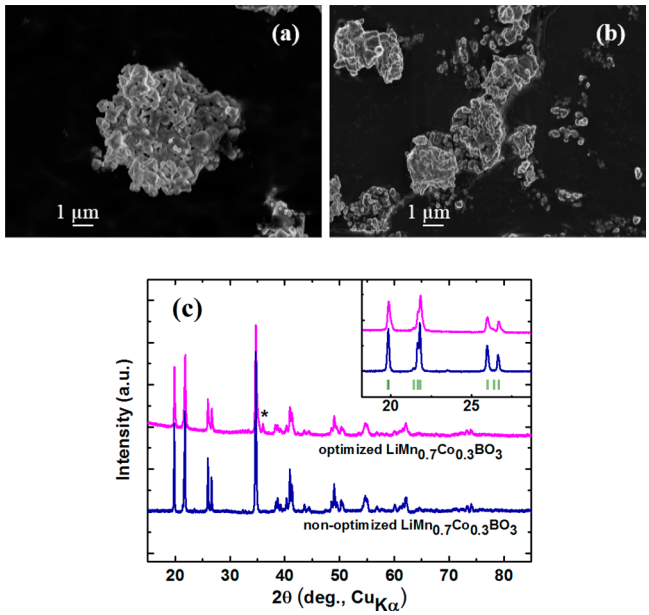

Figure 8. (a) SEM image of nonoptimized $LiMn_{0.7}Co_{0.3}BO_3$. (b) SEM image of optimized $LiMn_{0.7}Co_{0.3}BO_3$. (c) XRD patterns of optimized and nonoptimized $LiMn_{0.7}Co_{0.3}BO_3$ [*, $Co_3(BO_3)_2$].

parameters calculated suggest that there is probably less than 0.3 cobalt in the structure. This can come from the short duration of the second heat treatment, which does not allow total diffusion of the cobalt ion in the structure. This is confirmed by the presence of a $Co_3(BO_3)_2$ impurity. SEM images presented in Figure 8b show that agglomerates formed with the optimized synthesis are smaller than those with the initial one (1−5 vs 3−10 μm).

The first galvanostatic cycling curves of $LiMn_{0.7}Co_{0.3}BO_3$ obtained for the optimized and nonoptimized compounds are

DOI: 10.1021/acs.inorgchem.5b00260
Inorg. Chem. 2015, 54, 5273−5279

shown in Figure 9. The evolution of the specific reversible capacity upon cycling is also presented. Measurements were

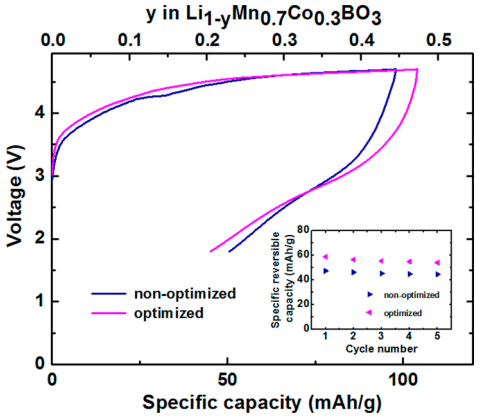

Figure 9. First galvanostatic charge−discharge curves at $C/20$ rate of $LiMn_{0.7}Co_{0.3}BO_3$. Inset: Evolution of the specific reversible capacity upon cycling between 1.8 and 4.7 V.

made at room temperature at a constant rate of $C/20$ between 1.8 and 4.7 V. The optimized compound shows better performances. Indeed, it has a higher reversible capacity: 59 mAh/g vs 48 mAh/g (+23%) with good stability up to five cycles. This probably comes from the smaller agglomerates obtained with this process, which allow better Li^+ diffusion during the discharge.

These performances should be improved with the development of in situ carbon coating during the synthesis. However, some attempts have been made with cellulose but without success because of the easy formation of cobalt metal during heat treatment at the temperature required for the formation of a conductive carbon coating especially under the reductive environment brought on by decomposition of the polymer. The introduction of carbon like Ketjen Black or VGCF during the second step, as was made by Yamashita et al. on the $LiCoBO_3$ compound,[8] should be possible, and some attempts are ongoing.

CONCLUSION

A complete solid solution of *m*-$Li(Mn_{1-x}Co_x)BO_3$ was synthesized for the first time. These compounds were obtained by a multiple-step process, with the formation of orthoborate $M_3(BO_3)_2$ (M = Mn, Co) essential to preventing the formation of metallic cobalt and Mn^{3+} during the heat treatment. Interestingly, the $C2/c$ space group previously reported for *m*-$LiMBO_3$ (M = Mn, Co) cannot describe *m*-$Li(Mn_{1-x}Co_x)BO_3$ compounds (with $x > 0$). The C2 space group fits with the extinction conditions observed in the ED patterns; however, XRD data are not sufficient to completely resolve the structure of these compounds. Neutron diffraction is planned and should help with the complete solution of the structure.

Each compound shows electrochemical activity with high polarization and limited reversible capacity. However, optimization of the synthesis allows one to obtain better performances with almost 60 mAh/g at the first discharge at $C/20$ rate with good stability up to five cycles for $LiMn_{0.7}Co_{0.3}BO_3$. However, its specific capacity can still be optimized. In particular, strategies based on in situ carbon coating and the reduction of the particle size may be profitable.

AUTHOR INFORMATION

Corresponding Author

*E-mail: jean-francois.colin@cea.fr. Phone: +33 (0) 4 38 78 34 91.

Author Contributions

The manuscript was written through contributions of all authors. All authors have given approval to the final version of the manuscript.

Notes

The authors declare no competing financial interest.

ACKNOWLEDGMENTS

We acknowledge the Commissariat à l'Energie Atomique et aux Energies Alternatives (CEA) for a Ph.D. grant. The authors thank Nathalie Diaferia for ICP measurements and Vincent Caldeira for SEM images.

REFERENCES

(1) Nanjundaswamy, K. S.; Padhi, A. K.; Goodenough, J. B.; Okada, S.; Ohtsuka, H.; Arai, H.; Yamaki, J. *Solid State Ionics* **1996**, *92* (1−2), 1−10.
(2) Masquelier, C.; Padhi, A. K.; Nanjundaswamy, K. S.; Goodenough, J. B. *Solid State Chem.* **1998**, *135*, 228.
(3) Ellis, B. L.; Lee, K. T.; Nazar, L. F. *Chem. Mater.* **2010**, *22*, 691−714.
(4) Padhi, A. K.; Nanjundaswamy, K. S.; Goodenough, J. B. *Electrochem. Soc.* **1997**, *144*, 1188.
(5) Seo, D.-H.; Park, Y.-U.; Kim, S.-W.; Park, I.; Shakoor, R. A.; Kang, K. *Phys. Rev. B* **2011**, *83*, 205127.
(6) Legagneur, V.; An, Y.; Mosbah, A.; Portal, R.; Le Gal La Salle, A.; Verbaere, A.; Guyomard, D.; Piffard, Y. *Solid State Ionics* **2001**, *139*, 37−46.
(7) Kim, J. C.; Moore, C. J.; Kang, B.; Hautier, G.; Jain, A.; Ceder, G. *J. Electrochem. Soc.* **2011**, *158*, A309−A315.
(8) Yamashita, Y.; Barpanda, P.; Yamada, Y.; Yamada, A. *ECS Electrochem. Lett.* **2013**, *2*, A75−A77.
(9) Afyon, S.; Mensing, C.; Krumeich, F.; Nesper, N. *Solid State Ionics* **2014**, *256*, 103−108.
(10) Yamada, A.; Iwane, N.; Harada, Y.; Nishimura, S.-i.; Koyama, Y.; Tanaka, I. *Adv. Mater.* **2010**, *22*, 3583−3587.
(11) Abouimrane, A.; Armand, M.; Ravet, N. *Proc. Electrochem. Soc.* **2003**, *201522*.
(12) Yamada, A.; Iwane, N.; Nishimura, S.-i.; Koyama, Y.; Tanaka, I. *J. Mater. Chem.* **2011**, *21*, 10690−10696.
(13) Belkébir, A.; Tarte, A.; Rulmont, A. *New J. Chem.* **1996**, *20*, 311−316.
(14) Tao, L.; Neilson, J. R.; Melot, B. C.; McQueen, T. M.; Masquelier, C.; Rousse, G. *Inorg. Chem.* **2013**, *52*, 11966−11974.
(15) Bondareva, O. S.; Simonov, M. A.; Egorov-Tismenko, Yu. K.; Belov, N. V. *Sov. Phys. Crystallogr.* **1978**, *23*, 269−271.
(16) Piffard, Y.; Rangan, K. K.; An, Y.; Guyomard, D.; Tournoux, M. *Acta Crystallogr.* **1998**, *C54*, 1561−1563.
(17) Tao, L.; Rousse, G.; Chotard, J. N.; Dupont, L.; Bruyère, S.; Hanzel, D.; Mali, G.; Dominko, R.; Levasseur, S.; Masquelier, C. *J. Mater. Chem. A* **2014**, 2060−2070.
(18) Lin, Z.; Zhao, Y.-J.; Zhao, Y. *Phys. Lett. A* **2012**, *376*, 179−184.
(19) Li, S.; Xu, L.; Li, G.; Wang, M.; Zhai, Y. *J. Power Sources* **2013**, *236*, 54−60.
(20) Kim, J. C.; Li, X.; Moore, C. J.; Bo, S.-H.; Khalifah, P. G.; Grey, C. P.; Ceder, G. *Chem. Mater.* **2014**, *26*, 4200−4206.
(21) Lee, Y.-S.; Lee, H. *J. Ceram. Process. Res.* **2012**, *13* (2), 237−240.

DOI: 10.1021/acs.inorgchem.5b00260
Inorg. Chem. 2015, 54, 5273−5279